Rhizomorph: The Coordinated Function of Shoots and Roots

BOSHENG LI, Purdue University, USA
JONATHAN KLEIN, KAUST, KSA
DOMINIK L. MICHELS, KAUST, KSA
BEDRICH BENES, Purdue University, USA
SÖREN PIRK, Adobe Research, USA
WOJTEK PAŁUBICKI, Adam Mickiewicz University, Poland

Computer graphics has dedicated a considerable amount of effort to generating realistic models of trees and plants. Many existing methods leverage procedural modeling algorithms – that often consider biological findings – to generate branching structures of individual trees. While the realism of tree models generated by these algorithms steadily increases, most approaches neglect to model the root system of trees. However, the root system not only adds to the visual realism of tree models but also plays an important role in the development of trees. In this paper, we advance tree modeling in the following ways: First, we define a physically-plausible soil model to simulate resource gradients, such as water and nutrients. Second, we propose a novel developmental procedural model for tree roots that enables us to emergently develop root systems that adapt to various soil types. Third, we define long-distance signaling to coordinate the development of shoots and roots. We show that our advanced procedural model of tree development enables – for the first time – the generation of trees with their root systems.

CCS Concepts: • **Computing methodologies** → **Modeling methodologies**.

Additional Key Words and Phrases: Botanical Tree Models, Vegetation Modeling, Natural Phenomena, Interactive Modeling, Root and Shoot System, Physics-based Modeling and Simulation

ACM Reference Format:
Bosheng Li, Jonathan Klein, Dominik L. Michels, Bedrich Benes, Sören Pirk, and Wojtek Pałubicki. 2023. Rhizomorph: The Coordinated Function of Shoots and Roots. *ACM Trans. Graph.* 42, 4, Article 59 (August 2023), 16 pages. https://doi.org/10.1145/3592145

1 INTRODUCTION

The ubiquitousness of vegetation in real scenes renders models of trees and plants an integral asset for applications in visual computing. Models of plants are used in settings as diverse as games and movies, architecture and urban planning, forestry and agriculture, and the training of autonomous agents or smart farming systems [Klein et al. 2023]. As the overall realism of virtual scenes increases across these domains, so do the requirements for the fidelity of plant models. This does not just include the visual aspects but also extends to the simulation of intricate biological and physical processes to drive the generation of plausible animations or to advance the understanding of a studied phenomenon, such as wildfires [Hädrich et al. 2021], erosion [Cordonnier et al. 2017], climatic gradients [Makowski et al. 2019; Pałubicki et al. 2022], and animal behavior [Ecormier-Nocca et al. 2021]. However, despite these advances, the development of complete trees, consisting of above-ground branching structures and their root systems, has not yet been modeled.

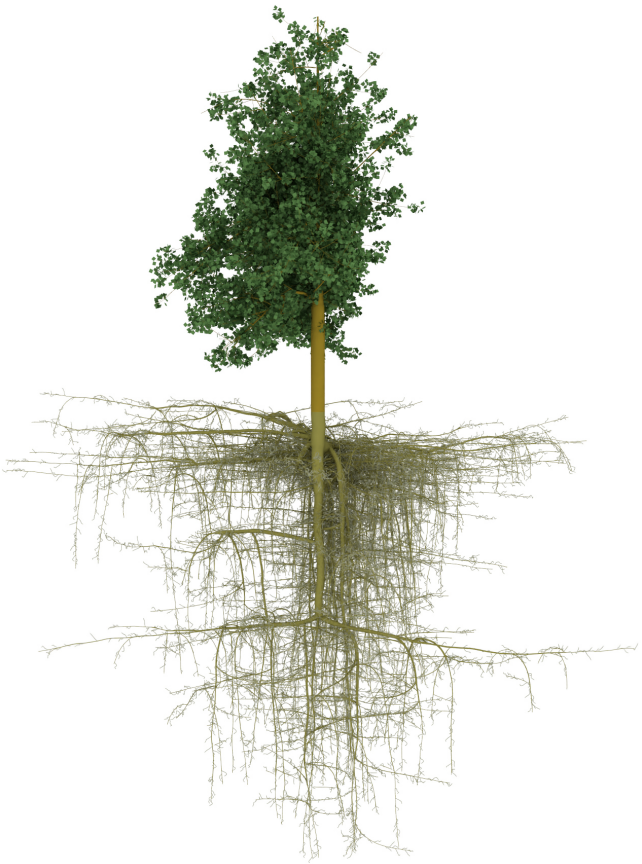

Fig. 1. A rendering of a simulated tree with our method. Our biologically-plausible model captures the coordinated development of shoot and root branches, as well as their interaction with the environment by taking up water and nutrients.

Arguably, in many situations root systems of trees may well be neglected. Roots are often not visually present and do not obviously

Authors' addresses: Bosheng Li, i2343@purdue.edu, Purdue University, 401 North Grant Street, West Lafayette, IN, 47907-2021, USA; Jonathan Klein, jonathan.klein@kaust.edu.sa, KAUST, Thuwal 23955, KSA; Dominik L. Michels, dominik.michels@kaust.edu.sa, KAUST, Visual Computing Center, Thuwal 23955, KSA; Bedrich Benes, bbenes@purdue.edu, Purdue University, 401 North Grant Street, West Lafayette, IN, 47907-2021, USA; Sören Pirk, soeren.pirk@gmail.com, Adobe Research, 345 Park Avenue San Jose, CA 95110-2704, USA; Wojtek Pałubicki, wojciech.palubicki@amu.edu.pl, Adam Mickiewicz University, Uniwersytetu Poznańskiego 4, 61-614, Poznań, Poland.

0730-0301/2023/8-ART59
https://doi.org/10.1145/3592145

contribute to what is visible to the observer. However, it is challenging to model them realistically for applications where roots are of main interest. This ranges from complex ground-root interactions to enhance the visual realism, e.g., for trees growing on rocky terrain or at slopes, to simulations of root systems for predicting tree development, e.g., in farming or utility planning scenarios. Roots grow in response to different soil types, according to the availability of resources (nutrients and water), and the overall development of trees. The complex interplay between root and shoot development leads to intricate geometric traits, which are difficult to model manually. Besides increasing the visual realism through the modeled roots, realistically simulating the growth of roots along with their resource uptake from the soil also enables modeling more realistic tree form in response to environmental conditions (e.g., for drought or nutrient availability).

A number of methods model root systems geometrically [Leitner et al. 2010; Měch and Prusinkiewicz 1996]. However, these methods either only model the root system in isolation, without root-soil interaction, or only use simplified geometry for representing root systems. To the best of our knowledge, root-soil interactions and the physically-plausible simulation of resource uptake for developmental tree models have not yet been studied.

In this paper, we aim to advance tree modeling in the following ways: first, we define a soil model based on a grid-based solver. The soil representation not only allows us to define different soil types and their properties (e.g., permeability and water capacity) but also to simulate the distribution of resource gradients for water and nutrients. Second, we define a novel developmental model for trees that are defined by a set of parameters that also enables modeling the specific morphology of developing roots. We abstain from a categorical description of roots (taproots, heart roots, lateral roots, etc.), but instead define our developmental model so as to express different root types emergently – roots grow based on species-specific characteristics and develop in response to different soil types and available resources.

Our framework allows us to interactively model the development of complete trees (above- and below-ground branching structures) and define the long-distance signaling between shoots and roots based on environmental stimuli (light, water, nutrients, and other soil properties). With this more complete approach to tree modeling, we can generate a range of results that could not be modeled before. Specifically, we show for the first time the whole 3D development of complex trees, including roots. As we model the interaction of roots and soil, our framework also allows us to model tree development in response to different levels of water and nutrient availability – trees in different soil conditions express various root architectures.

An example tree model generated with our framework showing a developed shoot and root system is shown in Fig. 1. In summary, the contributions of our method are as follows: (1) we propose a novel developmental model that also enables us to emergently simulate roots of different tree species in response to the soil model; (2) We model the long-distance signaling to coordinate the development of shoots and roots; (3) we propose a lightweight, dynamic soil model based on soil properties relevant to root development.

2 RELATED WORK

Early approaches modeled branching structures as rule-based algorithms [Honda 1971; Prusinkiewicz and Lindenmayer 1990], grammars [Aono and Kunii 1984], particles [Reeves and Blau 1985], and fractals [Oppenheimer 1986]. L-systems are one of the most prominent formal descriptions for modeling plant structures [Prusinkiewicz 1986] that have also been used for modeling roots systems [Leitner et al. 2010; Měch and Prusinkiewicz 1996]. Procedural modeling methods (parameterized algorithms) expand on the success of these early approaches by defining powerful mathematical models for phenomenological or self-organizing tree growth that can generate a large variety of tree architectures [Guo et al. 2020; Palubicki et al. 2009; Runions et al. 2007; Stava et al. 2014]. Only a few approaches exist to model root systems of trees [Tobin et al. 2007], Greene [1991] used voxels space automata for root-obstacle development simulation. However, existing approaches do not generate complete trees or root systems interacting with soil.

Sketch-based methods aim to facilitate the generation of tree models through user-defined gestures that are used to drive the procedural modeling of branching structures of trees [Chen et al. 2008; Okabe et al. 2007; Tan et al. 2008], plants [Anastacio et al. 2006] and flowers [Ijiri et al. 2006]. TreeSketch is an advanced approach for combing user-defined sketches with procedural modeling [Longay et al. 2012]. Moreover, sketches can also be used to define intermediate representations for tree modeling, such as envelope shapes [Benes et al. 2009], to guide the modeling process [Wither et al. 2009] or for guiding particle flows [Neubert et al. 2007]. These methods focus on the user interaction to generate the upper tree part and do not provide root systems.

With images and point clouds becoming common data modalities, researchers have attempted to reconstruct tree models from data. Various methods exist to reconstruct trees and foliage from multiple [Bradley et al. 2013; Neubert et al. 2007; Reche-Martinez et al. 2004] or single photographs [Quan et al. 2006; Tan et al. 2008], segmentation masks [Argudo et al. 2016], point clouds [Liu et al. 2021; Livny et al. 2011; Xu et al. 2007], time varying data [Li et al. 2013], and videos [Li et al. 2011]. More recently, it has also been recognized that neural networks can be leveraged as powerful function approximators to facilitate the reconstruction of tree models. While explicit tree geometry cannot yet directly be reconstructed with neural networks, methods use intermediate representations, such radial bounding volumes [Li et al. 2021] or branch parts [Liu et al. 2021] to reconstruct trees from images or point clouds. Due to the inherent difficulty of capturing roots, only a handful of approaches exist to reconstruct 3D models of roots through the structure from motion [Lu et al. 2021] or by obtaining a 3D model after excavating the root system [Ohashi et al. 2019].

Recently, researchers also simulated the biological development of plant models and their physical response to environmental factors. This ranges from methods that realize the dynamic development of tree models [Longay et al. 2012; Pirk et al. 2012a], the interaction of plants with their environment [Hädrich et al. 2017; Pirk et al. 2012b; Wong and Chen 2015], wind and tree interactions [Habel et al. 2009; Pirk et al. 2014; Quigley et al. 2018; Shao et al. 2021],

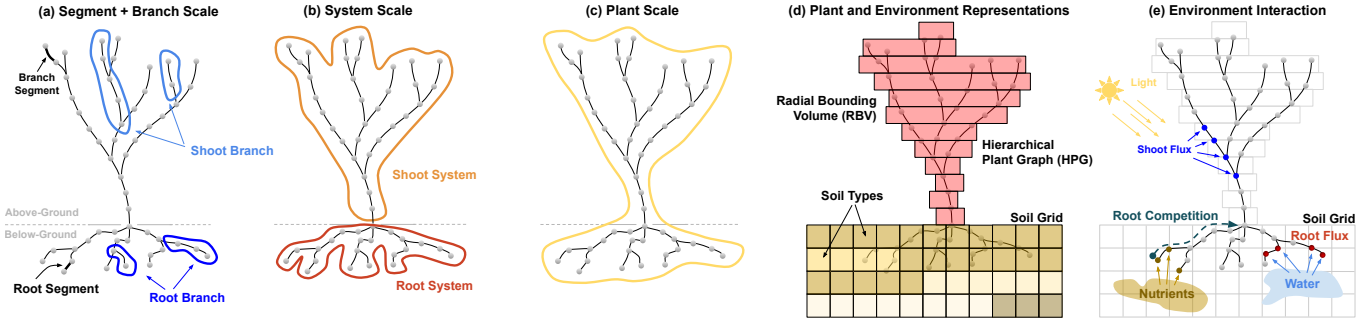

Fig. 2. Plants are represented as a hierarchical graph. (a): At its lowest scale, we define branch segments as nodes. Branch segments define whole root and shoot branches represented as nodes at the next scale. (b): At the third scale of the graph, we represent the shoot and the root systems as individual nodes. (c): The highest scale describes the whole plant. (d): The plant graph is embedded into representations of the soil and the atmosphere with a soil grid and a radial bounding volume. (e): Environmental stimuli of light, water, and nutrients are integrated into the plant graph as shoot flux, root flux, and root competition signal.

tree combustion [Pirk et al. 2017], the development of the cambium [Kratt et al. 2015], and even physical material properties based on FEM methods [Wang et al. 2017; Zhao and Barbič 2013]. Similar to these approaches, we aim to improve tree modeling by combining procedurally generated root and branching structures with a physics-based solver for soil.

Understanding the root systems is of central interest in agriculture and botany. Researchers not only study the function of root systems and their growth [Coutts 1987, 1989] but also their 3D distribution [Dobson et al. 1995] and how they vary for different tree species [Becker and Castillo 1990; Sutton 1980; Vercambre et al. 2003]. Furthermore, researchers are interested in understanding the morphology of roots [Busgen 2007; Cutler et al. 1990], how deep they grow [Gasson and Cutler 1990; Gilman 1990], and how far they spread around a tree [Hodgkins and Nichols 1977; Stone and Kalisz 1991; Stout 1956]. Roots can also cause damage to buildings and pipes [Biddle 2001], and they play a major role in maintaining the structural integrity of soil [Sutton 1991]. A survey on assessing and analyzing 3D architectures of root systems was provided by Danjon and Reubens [2008]. Our work is inspired by these approaches, but we focus on shape and appearance as an emergent phenomenon from interaction with the soil and nutrients.

3 OVERVIEW

Our main goal is to advance individual plant modeling by emphasizing the role of the coordinated development of the shoot and root (rhizae) shape (morph) – which leads to the name of our model *Rhizomorph*[1]. To this end, we carefully describe environmental stimuli and their integration into a long-distance signaling network representing plant development.

In our method, we have extended established approaches for generating realistic 3D geometries of botanical plants [Palubicki et al. 2009; Stava et al. 2014]. Plant models are represented by an acyclic *Hierarchical Plant Graph (HPG)* from which we obtain surface meshes representing the plant structure. The HPG has four scales:

[1]The term *rhizomorph* derives from Ancient Greek "rhíza" meaning "root" and "morphé" meaning "shape". It is commonly used in the context of branching and filamentous structures in fungi, and can be generalized to any type of root structures such as in botanical trees and plants.

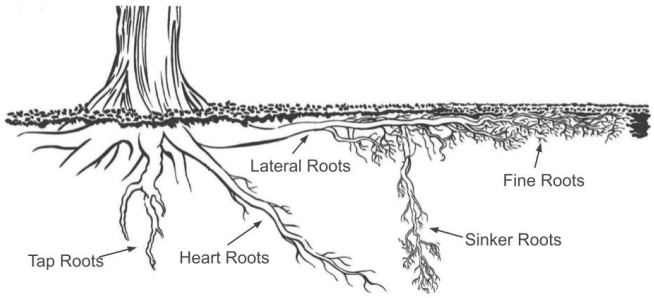

Fig. 3. Roots are commonly categorized as Tap Roots, Heart Roots, Lateral Roots, Sinker Roots, and Fine Roots (image adapted from [Plus 2023]).

segment, branch, system, and plant scale. At the lowest scale of the hierarchy, we describe information processing between plant segments representing organs such as buds, internodes, and leaves. The node attributes of the HPG store plant parameters such as organ state and size. The node attributes of the HPG are updated in a series of simulation steps representing plant development in our model. The computations for a single node may depend on attribute values of other nodes in the HPG, which then represent plant-internal signaling that coordinates the joint development of organs. At subsequent scales, we describe the signaling between branches, the shoot and root system, and the plant as a whole. The information propagation occurs both between nodes of a single scale as well as between different scales of the HPG (Fig. 2a-c).

We couple our plant model with a soil and atmospheric model. The soil model is defined by a set of coupled differential equations considering a 3D spatial domain represented by a discrete grid (soil grid). With this representation, our method is capable of expressing various types of soil with differing structural compositions and nutrient qualities, such as loam, sand, or humus. We define a lightweight atmosphere model allowing us to assess light availability using a discrete radial bounding volume (RBV) data structure [Li et al. 2021] (Fig. 2d).

Environmental information stored in the soil and atmospheric model is integrated into the developmental process of the plant represented by the HPG. We consider three distinct sources of environmental stimuli: light, water, and nutrients. Information about

light exposure of shoot segments is obtained from the atmospheric model and integrated into the HPG as an abstract plant signal called Shoot Flux (S_F). In contrast, water and nutrient availability for root segments is obtained from the soil model and integrated as Root Competition Signal (R) and Root Flux (R_F), shown in Fig. 2e. We compute updated values for all signals in simulation steps. A glossary for biological terminology is provided in the Appendix.

4 BIOLOGICAL BACKGROUND

The overall form of a plant is largely determined by the primary growth of organs at the tips of shoots and roots (apical bud). The relative development of shoots and roots is a response to environmental stimuli as well as genetic programming. Shoot and root systems perform different functions for the plant: shoots produce photosynthates by interacting with light, while roots take up water and nutrients. Since these systems integrate different resources necessary for plant development, their growth has to be coordinated according to the current requirements of the plant. Consequently, the spatial separation between shoot and root buds requires long-distance signaling to coordinate the growth of these two systems [Berleth and Sachs 2001; Leyser 2011]. Research in biology indicates that the majority of this signaling is mediated by hormones carried upstream or downstream through the plant vascular system. Other important signals include sugar produced in leaves by photosynthesis and nitrate directly obtained from the soil [Morris et al. 2017]. Shoot and root systems not only perform different functions for the plant, but the developmental processes controlling their form also differ significantly, as observed by research in biology [Puig et al. 2012].

Specifically, the root system, which is unique to land plants, is assumed to be one of the key factors that contributed to the overwhelming success of plants as an organism in evolution. Root form is highly dependent on the soil in which it is growing and can take on one of many possible configurations. In botany, a common categorization of root systems is in three classes: *Taproot System*, *Lateral Root System*, and *Heart (aka Oblique) Root System*. The taproot system is characterized by a prominent, vertically growing branch called a tap root. This root type is shared by all tree species and appears at the beginning of their development but is later usually outgrown by other root types. The lateral root system is characterized by a large number of *lateral roots* that grow close to the soil surface. The heart root system is made up of root branches that grow diagonally (*heart roots*), often into a spherical pattern. Other types of roots which are separately classified include *sinker roots* that can sprout vertically downwards from lateral roots. All the aforementioned types of roots can give rise to *fine roots*, which are much thinner and shorter in comparison but can directly absorb nutrients and water (Fig. 3).

The form of the whole root system is rarely directly observable by humans but, perhaps surprisingly, often differs significantly from the form of the attached shoot system of a plant. Consider the examples shown in Fig. 4.

5 MODEL

We introduce a plant growth model that describes environmental interaction with light, water, and nutrients. In the following sections, we introduce the hypotheses formalized in our model, the spatial domains of information transfer, and provide a definition of our complete plant model based on long-distance signaling and our soil model.

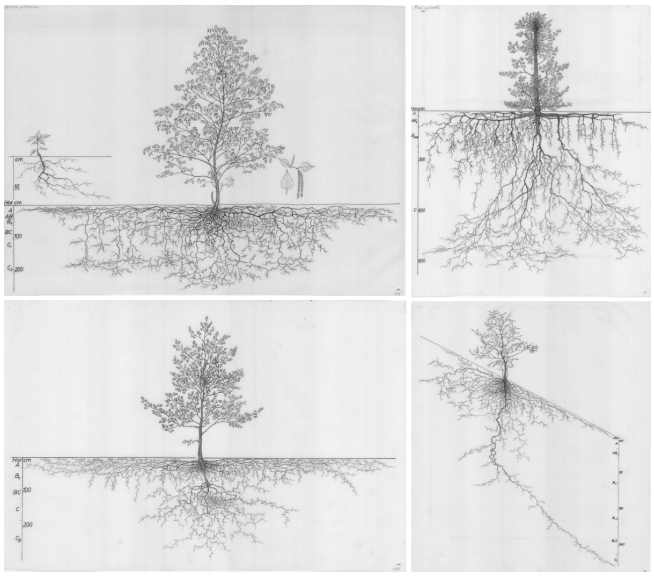

Fig. 4. Illustrations of root systems of the four tree species Betula Pendula (top left), Pinus Sylvestris (top right), Quercus Robur (bottom left), and Castanea Sativa (bottom right). The illustrations are courtesy of Wageningen University & Research - Image Collections.

5.1 Hypotheses

The construction of our plant model follows a phenomenological approach where we formalize a set of key biological hypotheses. We carefully selected a parsimonious set of assumptions to represent internal plant processes as well as plastic responses to environmental stimuli and their coordinated integration that represents development in our model. The key hypotheses are:

(1) Basipetal information transfer determines apical dominance (Organ Activation Signal) and apical control (Shoot Competition Signal); Eq. 3 and Eq. 4.
(2) Shoot branch growth is dependent on light availability (Shoot Flux Signal); Eq. 8.
(3) Root branch growth is dependent on acropetal water uptake (Root Flux Signal); Eq. 9.
(4) Local nutrient gradients and shoot-root ratio specify root branch development (Root Competition Signal); Eq. 6.
(5) External resource acquisition leads to growth potential (Vigor Signal) for organ development dependent on size; Eq. 15.
(6) Organs have maintenance and growth requirements dependent on their size (Organ State); Eq. 2
(7) The coordinated shoot and root information processing determine root-branch competition (long-range signaling); Eq. 10 - Eq. 12
(8) Nutrients are advected by water; Eq. 30.

Hypotheses (1)-(7) apply to the plant model, whereas hypothesis (8) to the soil model. The formalization of (1)-(7) is based on discrete

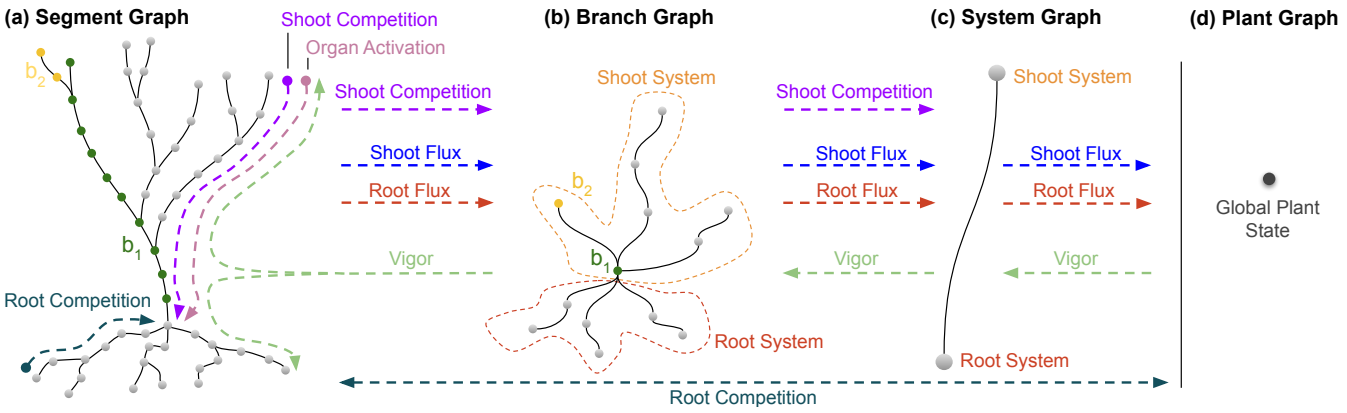

Fig. 5. Signal flow in the Hierarchical Plant Graph (HPG) occurs at the segment scale (a) for the Root Competition, Shoot Competition, and Organ Activation signals. Shoot Competition, Shoot Flux, and Root Flux signals are passed up the hierarchies of the HPG until the plant scale (b-d). At the plant scale, these signals are transformed into a Vigor signal, which is propagated downwards to the segment scale, until each segment is allotted an amount of vigor. The Root Competition signal is directly aggregated at the plant scale from the segment scale. The upwards and downwards propagation of signals at the different scales of the HPG represents long-distance signaling in our model.

graph node computations, whereas for (8), we rely on a set of partial differential equations resolved in a 3D domain. We couple both models by embedding the discrete soil grid and HPG in the same continuous Euclidean space.

5.2 Spaces

The main challenge in describing plastic plant development is to express the joint action of environmental and intrinsic processes. We express plant developmental dynamics using a hierarchical tree graph of connected nodes to accommodate this challenge. A hierarchical graph allows propagating signals both within a single scale as well as between scales. At the lowest scale of the hierarchy, nodes $n \in N$ represent segments of shoot or root branches (Fig. 5a). At the next higher scale, nodes $b \in B$ represent branches of the shoot or root (Fig. 5b). At the following scale, nodes $s \in S$ represent the shoot and root system (Fig. 5c), and, finally, node $p \in P$ represents the whole plant system (Fig. 5d). Long-distance signaling that controls local developmental decisions is passed on at the segment scale, while signals that carry global developmental decisions are passed across the hierarchy. Each node is a data structure defined by a number of attributes (Tab. 1 and Appx. 9: List of Symbols).

Our soil model uses a 3D uniform grid that spatially discretizes the 3D domain of the partial differential equations. Each grid cell stores information about soil attributes such as growth resistance δ, water capacity c, water permeability p, as well as variables water w and nutrients ν representing soil dynamics. The atmosphere in our model is represented by a Radial Bounding Volume (RBV) data structure which is used to obtain estimates for light exposure (q) of plant organs [Li et al. 2021]. The atmospheric model also stores information for the temperature T in a given simulation step as specified directly by the modeler.

5.3 Tree Model

The HPG is composed of nodes at different scales. At the segment scale, nodes store values in attributes to generate the geometric shape of the plant and to represent the physiological plant state.

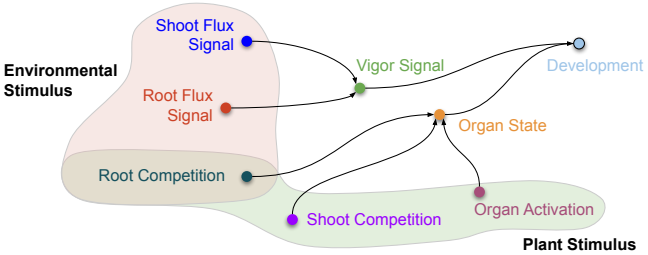

Fig. 6. In our model, the information processing of plants is encapsulated through the interaction of a number of signals. Shoot and Root Flux signals represent light and water stimuli, whereas Shoot Competition and Organ Activation signals express genetic programming. The Root Competition signal has a dual role in our model. All five signals are then aggregated by propagation through the HPG to two higher-level signals. The Vigor signal represents the growth potential of organs, whereas the Organ State signal represents the developmental requirements of organs. Vigor and Organ State signals together define development in our plant model.

Nodes belonging to the shoot system have different attributes compared to nodes belonging to the root system. Both types of nodes share the attributes of position x, diameter d, length l, bud number N_b, vigor V, optimal growth direction g, and orientation o. Shoot nodes also possess the attributes Shoot Flux Signal S_F, Activation Signal A, leaf number N_l. Root nodes contain the attributes Root Flux Signal R_F and Root Competition Signal R (Tab. 1).

5.3.1 Long-distance Signaling. The essence of our method is the node attribute update computation which represents signaling action in plants. We distinguish node computations that initially depend on data stored in the soil or atmosphere model such as Shoot Flux S_F and Root Flux R_F Signals, and node computations that solely depend on node attribute values. The shoot competition S, root competition R, and activation A signals represent plant internal information processing (Fig. 6). In our model, we update these variables in a sequential manner.

First, we compute the organ state $O(n_i) = (G_i, M_i, A_i, S_i)$ for each node $n \in N$. The organ state represents information about how much vigor V is required for maximum growth G and maintenance M, as well as signals A controlling bud activation and S controlling overall growth of child branches (Fig. 6). For all apical nodes of the shoot system of the HPG, we initialize organ state variables in the following way,

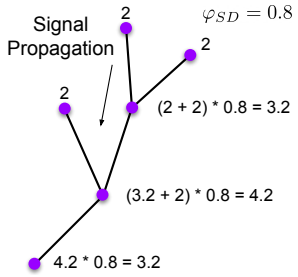

$$G_i^{(apical)} = shoot_g(l_i \cdot d_i + N_l \cdot \mu_l), \quad (1)$$

$$M_i^{(apical)} = l_i \cdot d_i, \quad (2)$$

$$A_i^{(apical)} = (G_i + M_i) \cdot \varphi_{ADD}, \quad (3)$$

$$S_i^{(apical)} = (G_i + M_i) \cdot \varphi_{ACD}, \quad (4)$$

where $shoot_g$ is the overall growth rate of the shoot system computed at each previous simulation step (Eq. 16, in the first iteration we initialize this variable with a default value) and φ_{ADD} φ_{ACD} global coefficients describing the overall inhibition capability of apical nodes of a plant species in regard to bud activation and internode growth. For root nodes the maintenance requirement M is computed exactly as for the shoots, but the maximum growth requirement is defined by

$$G_i^{(apical)} = root_g \cdot (\frac{1}{\delta})^{\varphi_{RG}}, \quad (5)$$

where φ_{RG} is a parameter describing how quickly a root can grow through the soil, $root_g$ the overall growth rate of the root, and δ the growth resistance of the soil. In addition, we also initialize for the root node a root competition signal R as

$$R_i^{(apical)} = \nu \cdot G_i + M_i. \quad (6)$$

Once all apical nodes have been initialized, we accumulate the maintenance requirement M, maximum growth requirement G, shoot competition signal S and the root competition signal R to the shoot and root base nodes until the total amount of maintenance, growth requirement and root competition signal is stored there. In the inset figure, we show how we accumulate values R, S and A at bifurcations and scale them with a coefficient ($\varphi_{SD} < 1$) that represents signal decay. Light exposure values L are used to compute the Shoot Flux signal S_F for each node of the HPG at the segment scale. We use the local light availability $L(n_i)$ for node i to compute S_F:

$$L(n_i) = \int_\Omega L_j(\omega_j)\, \mathrm{d}\omega_j, \quad (7)$$

$$S_F = f_\sigma(L(n_i)) \cdot \max_L, \quad (8)$$

where $\max_L$ denotes the maximum light availability that can be transformed into Shoot Flux S_F, $L_i(\omega_j)$ the incoming light from direction ω_j, Ω a sphere, and f_σ is the sigmoid function. While we calculate the integral for apical nodes, we also compute the optimal growth direction γ. This direction is selected to point to the location of the highest light availability on the sphere Ω [Palubicki et al. 2009]. Then the Shoot Flux S_F is accumulated at nodes of each higher hierarchy until we obtain the total Shoot Flux at the plant scale.

Table 1. Dynamic Parameters: node attribute values are calculated at each simulation step. They represent the shape and physiological information about plant segments. Most attributes are shared between shoot and root nodes (indicated by check marks), but some differ (indicated by the minus sign). The symbols refer to: position (x), diameter (d), length (l), bud number (N_b), leaf number (N_l), vigor (V), optimal growth direction (g), orientation (o),Shoot Flux Signal (S_F), Activation Signal (A), Root Competition Signal (R), and Shoot Competition Signal (S)

Node	x	d	l	N_b	N_l	V	g	o	S_F	A	R_F	R
Shoot	✓	✓	✓	✓	✓	✓	✓	✓	✓	✓	-	-
Root	✓	✓	✓	✓	-	✓	✓	✓	-	-	✓	✓

Similarly to the calculation of the Shoot Flux S_F, we also compute the Root Flux R_F for all nodes of the root. However, instead of computing light availability $L(n_i)$ using the RBV, we use the water value w stored in the soil grid cell (i, j, k), where the root node is located. Again, we use the notion of a maximum water availability $\max_W$ that can be transformed in Root Flux:

$$R_F = f_\sigma(w_{ijk}) \cdot \max_W. \quad (9)$$

Similar to the Shoot Flux, the Root Flux R_F is accumulated at nodes of each hierarchy until the total Root Flux is computed at the plant scale. Once the total Shoot and Root Flux are obtained, we compute the total vigor V^{plant}, which represents the available growth potential for the plant:

$$V^{\text{plant}} = \min(R_F^{\text{root}}, S_F^{\text{shoot}}). \quad (10)$$

This expresses water- or light-limited computation of vigor. In case $R_F < S_F$, the water uptake is limiting overall plant growth, while in the converse case light is limiting overall plant growth. We then compute the Vigor V^{shoot} available for the shoot system:

$$V^{\text{shoot}} = V^{\text{plant}} \cdot \frac{M^{\text{shoot}}}{M^{\text{shoot}} + M^{\text{root}}}, \quad (11)$$

where M denotes the vigor required for organ maintenance. The Vigor V^{root} is equal to $1 - V^{\text{shoot}}$. In our HPG we define two base nodes at segment scale for the root and shoot system which are connected to each other. Then, we calculate the Vigor v_b for the base nodes of the shoot and root. The base nodes are treated separately from all other nodes:

$$V_b = V^{\text{plant}} \frac{M_b + G_b}{M_b + G_b + \sum_{c \in C}(M_c + G_c)}, \quad (12)$$

where $c \in C$ are the directly connected nodes of the base node b. Once we have computed the vigor for the base nodes we propagate vigor values upwards from the shoot base node to the apical nodes of the shoot system. At each branching point we determine how much vigor is distributed towards the next node of the current branch (V_m) and how much to the node of the child branch (V_c) based on

the vigor of the parent node (V_p):

$$\varphi_{AC} = min(\lambda \cdot e^{-\varphi_{AF} \cdot \rho \cdot \text{shoot}_g}, 1)\,, \tag{13}$$

$$V_m = V_p \cdot \frac{\varphi_{AC}(S_m)}{\varphi_{AC}(S_m) + (1 - \varphi_{AC})(S_c)}\,, \tag{14}$$

$$V_c = (V_p - V_m)\,. \tag{15}$$

where φ_{AC} corresponds to the weight λ used in [Palubicki et al. 2009], but instead of a user specified value it is a derived value based on a tree age factor parameter φ_{AF}, the age of the tree ρ, and the shoot growth potential shoot_g. This means that as the tree ages in our simulation, the weight to distribute vigor decreases. Consequently, the older the tree becomes the smaller the inhibition of growth on child branches gets.

5.3.2 Development. Once the node updates have been computed, we update the HPG to express the developmental changes of the plant. First, we calculate the growth potential of the shoot $shoot_g$ and root $root_g$. These variables represent the overall growth potential of the shoot and root system:

$$\text{shoot}_g = \frac{V^{\text{shoot}}}{M^{\text{shoot}}}\,, \tag{16}$$

$$\text{root}_g = \frac{V^{\text{root}}}{M^{\text{root}}}\,. \tag{17}$$

Next, we determine which branches should be pruned from the shoot system of the HPG at the branch scale. We remove the branch from the HPG if the following inequality is true:

$$\frac{S_f^{\text{branch}}}{l^{\text{branch}}} < \varphi_{PT}\,, \tag{18}$$

where l^{branch} denotes the total length of a branch. We perform this test for all branch nodes of the branch graph. Then for all nodes of the segment graph of the shoot system, we compute potential internode extension. This is calculated using a plant-specific parameter $plant_l$, which defines the maximum length of internodes as a function of plant age following [Stava et al. 2014]:

$$l_i = (G_i - M_i) \cdot \text{plant}_l(\text{age}). \tag{19}$$

The direction of internode extension is defined by weights and phototropism parameters following the method from [Palubicki et al. 2009]. The direction of extension of an internode is the sum of three weighted vectors: the previous direction, the optimal growth direction obtained when calculating light availability (weight φ_{PT}), and a tropism vector (weight φ_{GT}). For all nodes that have a number of dormant buds attributed to them, we compute if a bud activates and a new node is attached to the segment graph. We compute the probability that a bud activates as:

$$P_A(sb_j) = e^{A_i} \cdot \text{shoot}_g \cdot \frac{T - \min_T}{\max_T - \min_T} \left(\frac{V_i}{d_i}\right)^{\varphi_{BA}}\,, \tag{20}$$

where $\min_T$ and $\max_T$ denote the lower and upper limit of the temperature range in the climate model, and φ_{BA} is a modulator of bud activation probability representing a plant species preference for activation, and sb a bud attached to a node. Please note that in the implementation we clamp differences with 0 to avoid negative probabilities. Each new apical node of the HPG may generate a number of dormant buds that may develop later in the simulation into new nodes. The number of buds and leaves as well as their arrangement on a shoot branch follows [Stava et al. 2014], but in contrast to the original approach, we use the allotted vigor V_d of nodes to compute varying instead of constant numbers of buds for apical nodes:

$$N_b(\text{bud}_i) = V_d^i / G_i \cdot \varphi_{\text{NLB}}\,. \tag{21}$$

We update root node attributes analogously to the shoot nodes with several exceptions. First, we compute the extension of internodes of the root system by taking into account the growth resistance of the soil δ (described in Sec. 6):

$$l_i = (G_i - M_i) \cdot \frac{\text{plant}_l}{\delta}\,. \tag{22}$$

Second, the change in diameter is calculated according to the pipe model introduced by Shinozaki et al. [1964]. Third, the extension direction of new root internodes is calculated by computing the optimal growth direction γ. We sample the local soil grid cell of a node and set its orientation pointing to the highest amount of nutrients to compute γ. Please note that water may control root branch growth direction indirectly by advecting nutrient concentrations in the soil. We also employ a user-specified tropism vector τ and the previous growth direction. These three vectors are scaled by weight ζ for tropism and η for growth direction to weigh their relative contribution to determine the root orientation (see [Palubicki et al. 2009] for more details). Contrary to the shoot nodes, the root nodes select a tropism vector locally as controlled by the probability $P(n_i)$ to switch between lateral and vertical tropism vectors:

$$P_T(n_i) = \varphi_{\text{ST}} \cdot \varphi_{\text{STD}}^{d(i,b)}\,, \tag{23}$$

where φ_{ST} denotes a user parameter controlling a global probability to switch tropism (ST), φ_{STD} a second probability derived from the graph distance (STD) between current node i and the base node b. Consequently, the further away a node is from the base node, the less likely it will switch tropism vectors. Finally, the formation of new root branches, contrary to the shoot branching, depends on the Root Competition signal R as well as a branching strength φ_{BS} to account for the effects of nutrients:

$$P_{RA}(rb_i) = R_i \cdot A_i \cdot \text{root}_g \cdot \varphi_{BS}\,. \tag{24}$$

Altogether, this defines a single step in the simulation of our plant model.

6 SOIL MODEL

Roots grow by absorbing water w and nutrients ν from the soil. Root development is affected by soil growth resistance. In our model, we describe soil by three static soil properties: (1) the growth resistance of the soil $\delta : \Omega \rightarrow \mathbb{R}^+$, (2) the capacity to store water $c : \Omega \rightarrow \mathbb{R}^+$, and (3) the soil permeability $p : \Omega \subseteq \mathbb{R}^3$. The soil domain Ω is a 3D space where soil properties are defined for each position.

The changes in w are modeled by the following equation:

$$\frac{\partial w}{\partial t} + \nabla \cdot \boldsymbol{j} = \mathcal{S}\,, \tag{25}$$

where t is the time, $\mathcal{S}$ is a source/sink term and $\nabla \cdot \boldsymbol{j}$ is the divergence of the water flux. The flux consists of multiple components:

$$\boldsymbol{j} = p \cdot (\boldsymbol{j}_{\text{diff}} + \boldsymbol{j}_{\text{grav}})\,, \tag{26}$$

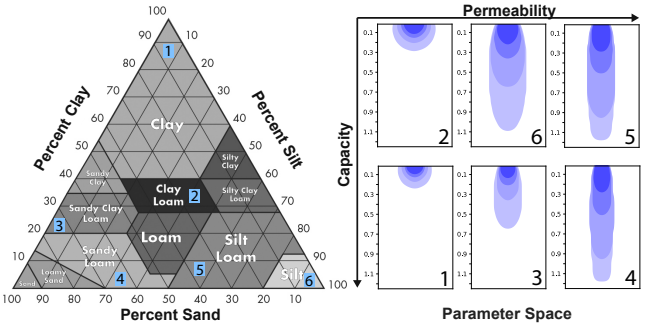

Fig. 7. The soil texture triangle chart is used for the classification of different soil types based on their composition of loam, clay, silt, and sand. Our soil model based on permeability (left to right) and water capacity (top to bottom) can express varying infiltration and drainage patterns as indicated by the blue contours. The blue color indicates the time (light is a longer simulation) and the vertical extent of the contour indicates the depth to which 80% of the water infiltrated. Based on these water flow properties, we can map our soil simulation to soil types such as clay (1), clay loam (2), sandy clay loam (3), sandy loam (4), silt loam (5), and silt (6).

where the permeability p at each position is used as a scaling factor for the fluxes. A permeability of zero, therefore, acts as an obstacle to the water flux. The flow of water due to diffusion is denoted by $\boldsymbol{j}_{\text{diff}}$. Different regions of the soil may have varying capacities c for storing water. Therefore, the relative water content is computed as:

$$\alpha = \frac{w}{c}\,. \tag{27}$$

For numerical stability, water capacity is always greater than zero. Then, the diffusion flux is relative to the negative gradient of the water content times the global diffusion strength $f_{\text{diff}} \in \mathbb{R}$:

$$\boldsymbol{j}_{\text{diff}} = -\nabla\alpha \cdot f_{\text{diff}}\,. \tag{28}$$

Note that for appropriate scaling and homogeneous capacity, this simplifies to $\boldsymbol{j}_{\text{diff}} = -\nabla w$. The gravity flux $f_{\text{grav}} \in \mathbb{R}^3$ is:

$$\boldsymbol{j}_{\text{grav}} = f_{\text{grav}} \cdot w\,. \tag{29}$$

Water is the dominant medium through which nutrients may be transported in the soil. In our model, we account for the advection due to gravity as well as diffusion:

$$\frac{\partial v}{\partial t} + \nabla \cdot (\boldsymbol{j} \cdot v) = 0\,. \tag{30}$$

Since soil permeability and capacity control water flow, the transport of nutrients is also affected by the soil properties. A summary of the used symbols of our soil model can be found in Tab. 2.

Mapping to Soil Types. Agriculture often classifies soils by using the soil texture triangle chart (Fig. 7, left), which describes soil types in terms of proportions of sand, clay, loam, and silt. Our soil model is based on the static soil properties of growth resistance δ, permeability p, and water capacity c, as well as dynamic soil properties of water w and nutrients v. It has been observed that different soil types have different hydraulic properties [Groenendyk et al. 2015]. For example, water in sandy soil infiltrates quickly, whereas in clay the flow is very slow. We demonstrate the capabilities of our method to simulate different hydraulic properties of soil in Fig. 7 (right).

Table 2. Soil parameters used in our model.

Symbol	Name	Units
t	Time	1 h
x	Position	1 m
Ω	Soil Volume	1 m
δ	Growth Resistance	1
p	Permeability	1 m/h
c	Capacity	unit/cm^3
w	Water	unit/cm^3
v	Nutrients	unit/cm^3
f_{diff}	Diffusion force	1
f_{grav}	Gravity	1
$\mathcal{S}$	Source / Sink	unit/cm^3
Δx	Voxel Size	1 m
Δt	Time Step	1 h

We simulate a slower infiltration of water by specifying low permeability values p and fast infiltration of water with higher values (e.g., sandy types of soil). The index numbers in Fig. 7 correspond to well-known types of soil and their hydraulic properties. In addition to the various soil types shown in the soil triangle, soils are often heterogeneous. For example, rocks of various sizes may be embedded in the soil, which affects water flow. Another factor might be nutrient-rich regions e.g., due to decomposing animal cadavers. To account for this heterogeneity, we employ 3D noise functions to control the placement of regions with permeability $p = 0$ (rocks) or sources of nutrients v. Specifically, we used the following parameter values for water capacity C and permeability P in the simulation results shown in Fig. 7: (1) C = 10, P = 0.0015, (2) C = 5, P = 0.0015, (3) C = 75, P = 0.033, (4) C = 150, P = 0.5, (5) C = 100, P = 0.5, (6) C = 50, P = 0.033.

7 IMPLEMENTATION

We have implemented our interactive standalone framework with C++, OpenGL, GLSL, and Vulcan with OptiX as the rendering engine. We also used CUDA to speed up numerical calculations. All results were generated on a computer with an RTX 3090 (24GB), an Intel ® i9-10850K processor, and 32GB of memory.

Discretization. At the beginning of each simulation step, we first update the temperature value for the atmospheric model. Then we compute the changes of water w and nutrients v. The soil volume is discretized into voxels with equal size δx in each dimension. Gradients for the diffusion flux j_{diff} (Sec. 6) are computed using the simple finite difference scheme. We use the Lax-Wendroff scheme to calculate advection Eq. 30. Time integration δt is performed using the Forward-Euler method. We use absorbing boundary conditions for the bottom and blocking boundary conditions where the permeability is set to zero of the soil grid. We compute the absorbing boundary conditions to modulate the water amount in voxels using: $w_i^{t+1} = w_i^t \cdot a_i$, with $a_i \in [0..1]$ with decay factor a_i of:

$$a_i = 1 - \exp\left(\frac{i}{0.2 \cdot \text{width}^2}\right). \tag{31}$$

For the absorbing boundary conditions, we use a width of five. We compute 24 iterations with our Lax-Wendroff scheme and 50 iterations for the diffusion integration for each plant simulation step (Alg. 1, lines 3-4).

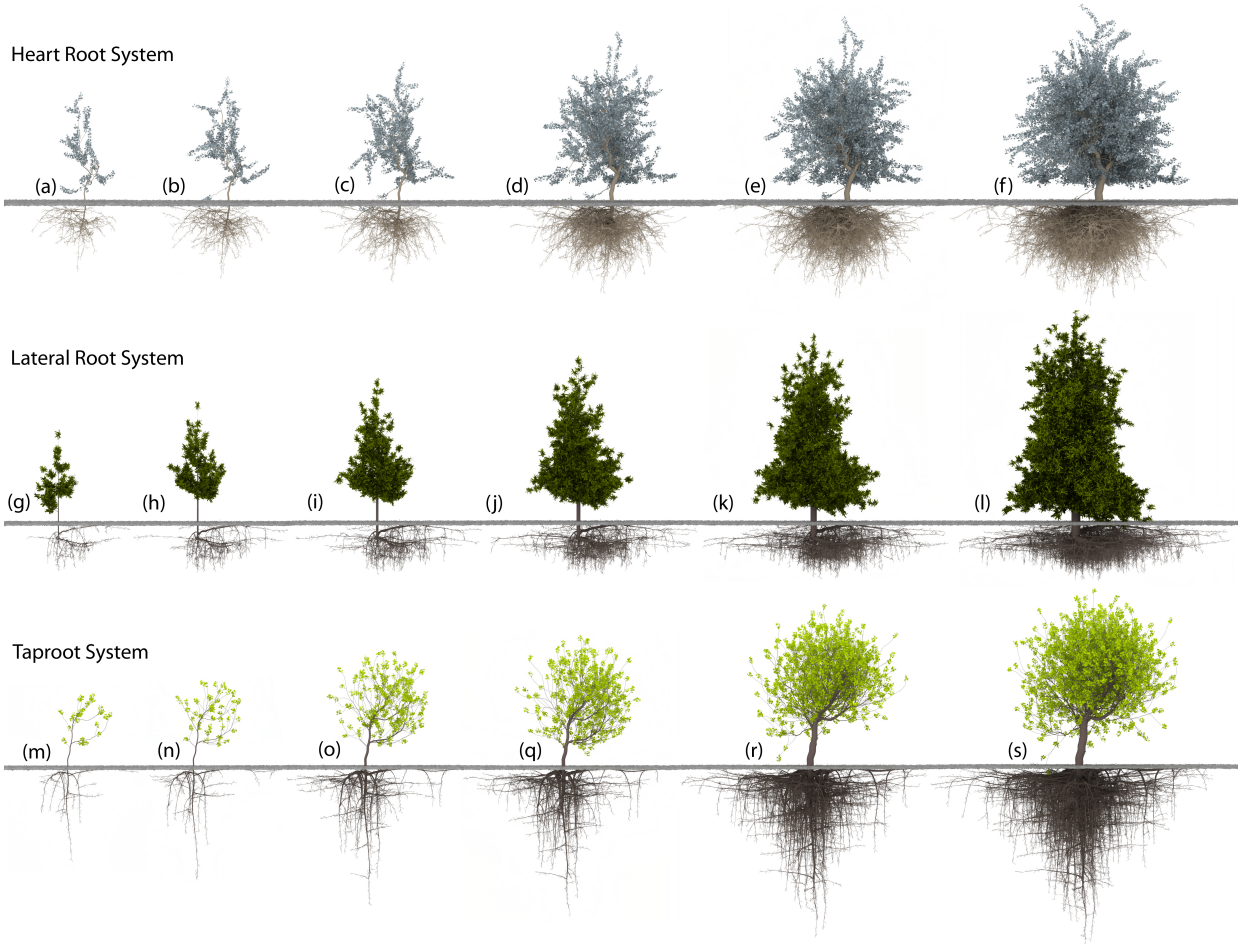

Fig. 8. Developmental progression of different tree species and their root systems. Different tree species tend to develop diverse root systems, such as the heart root system (a)-(f), the later root system (g)-(l), and the taproot system (m)-(s). Please note that the development of the root system is not linearly proportional to the development of the shoot system. In the early growth stages, the root systems develop faster.

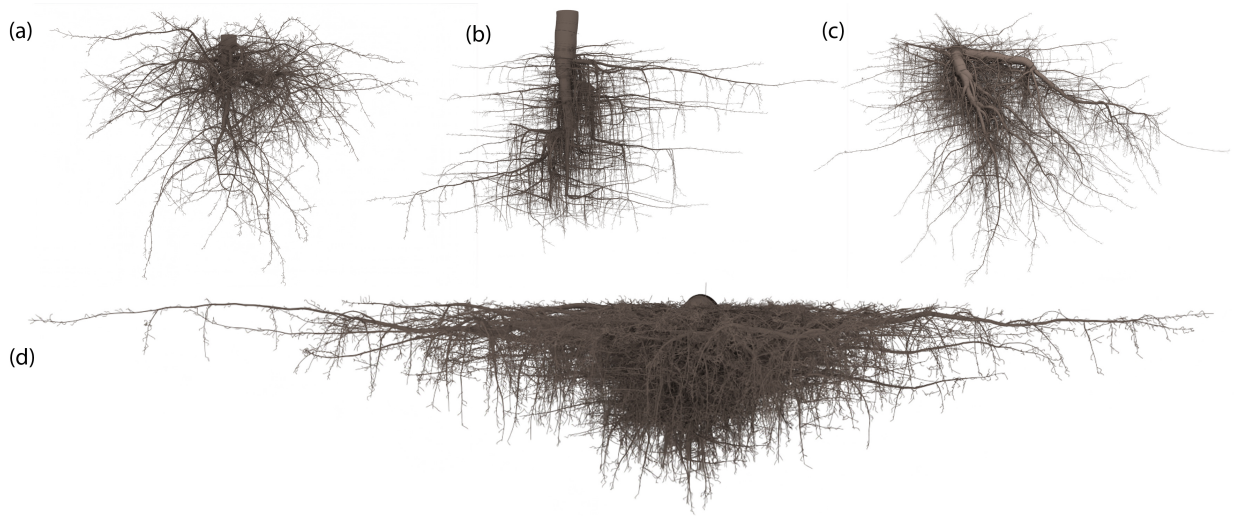

Fig. 9. As roots interact with the environment, our method enables the generation of diverse root systems. Commonly known root types (tap, lateral, heart, sinker roots) emergently develop while trees grow and interact with the soil. Here we show a heart root system (a), a taproot system (b), lateral root system with sinker roots (d). Different soil types cause trees to adapt their root system, which can lead to asymmetrically developed roots (c).

ALGORITHM 1: Overview of our numerical procedure.

Input: Current system state.
Output: Updated system state.
1 **Procedure:**
2 Update temperature values T in atmosphere model (Sec. 5.2).
3 **for each** $\gamma \in \Gamma$ **do**
4 | Compute water w and nutrient changes v for each soil
5 grid cell γ (Sec. 6).
6 **for each** $n \in N(apical)$ **do**
7 | Initialize growth G, maintenance M, root signal R, shoot signal S and activation signal A(Eqs. 1-6).
8 **for each** $n \in N$ **do**
9 | Accumulate maintenance M, maximum growth G, root signal R, shoot signal S and activation signal A horizontally through the HPG (Sec. 5.3.1).
10 **for each** $n \in N$ **do**
11 | Compute light availability L for each node n (Eq. 7)
12 | Compute S_F, R_F (Eq. 8, 9).
13 **for each** $(n, b, s) \in (N, B, S, P)$ **do**
14 | Accumulate S_F and R_F vertically through the HPG.
15 **for each** $(n, b, s) \in (N, B, S, P)$ **do**
16 | Compute V and propagate vertically (Eqs. 10, 11) and
17 horizontally (Eqs. 12-15) through the HPG.
18 **for each** $(n, b) \in (N, B)$ **do**
19 | Compute growth rates for shoot and root (Eqs. 16, 17).
20 | Prune branches (Eq. 18).
21 | Compute internode elongation and
22 radial extension (Eq. 22).
23 | Compute node tropism (Eq. 23).
24 | Activate dormant buds (Eq. 20).
25 | Compute bud number for nodes (Eq. 21).
26 **end**

Tree Simulation. Once the water w and nutrient v values have been updated, we initialize the organ state variable G and M for all apical nodes of the HPG (Alg. 1, lines 5-6). Then, we accumulate values M for all non-apical nodes using downwards propagation for the shoot and upwards propagation for the root (Alg. 1, lines 6-7). Next, we compute the light availability (Alg. 1, line 12) for each node of the segment graph by numerical integration and compute the Shoot Flux S_F and Root Flux Signals R_F (Alg. 1, lines 14-15). After this step, we propagate vigor values V vertically and horizontally in the HPG (Alg. 1, lines 16-18). Once the vigor values are allotted to all nodes, we perform pruning at the branch scale, calculate the internode elongation and radial extension, buds activation, and the addition of new buds at segment scale, (Alg. 1, lines 19ff.).

8 RESULTS AND EVALUATION

Our model depends on a number of parameters, and we aim to carefully explore different parameter settings through numerous examples. A tree model emerges through the interaction of the different components of the HPG. We simulate different root types, such as lateral or sinker roots, and their interaction with the soil. We also use the information gathered by the root system and show how it affects the upper part of the tree. Simultaneously, we propagate the information from the crown down to the root system.

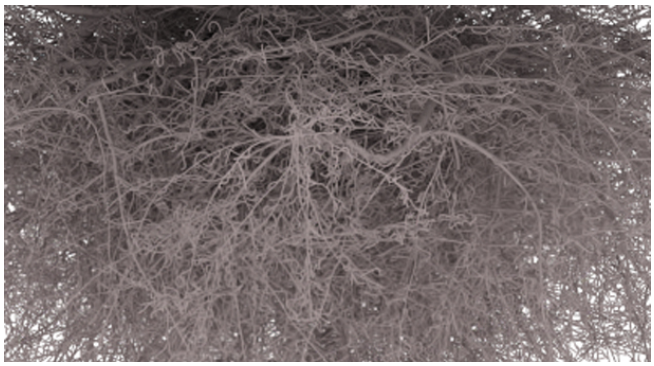

Fig. 10. A close-up of a fully developed root system of the tree shown in Fig. 8f. Our method is able to generate highly complex root systems, also including *fine roots*.

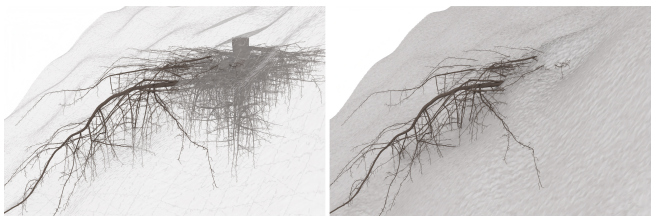

Fig. 11. Our method enables simulating root-soil interactions, and root systems can automatically adapt to different soil configurations. In this example, a root system has adapted to a mountain slope and grew out of the soil (left), resulting in visible roots on top of the soil (right).

8.1 Results

In Fig. 8, we show the temporal progression of plant growth from sapling to mature trees for three different species. We selected a parameter value configuration to model a heart (a-f), a lateral (g-l), and a taproot system (m-s). To model a heart root system, we choose a small value for the tropism weight ζ to compute the extension of an internode. This will emphasize root growth for optimal growth directions. While the lateral and taproot systems are modeled by choosing high or low values for φ_{ST} together with a high value for the tropism weight ζ, respectively. This emphasizes switching between lateral and/or vertical root branch growth.

In Fig. 9, we show detailed close-ups of two heart root systems (a), a taproot (b), an asymmetrically developed heart root system, and a dense lateral root system (d). In Fig. 10, we show a close-up rendering of a heart root system from a bottom perspective showcasing the geometric intricacy and complex architecture. We also explore the parameter space of our model by selecting parameter values to model 5 distinct species of trees. In Fig. 12, we show renderings of a simulated maple tree grown on a slope (a), an apple tree grown next to a low-permeability region (b), a young oak with a deep taproot (c), a poplar (d), and a cherry tree forming a wide lateral root system

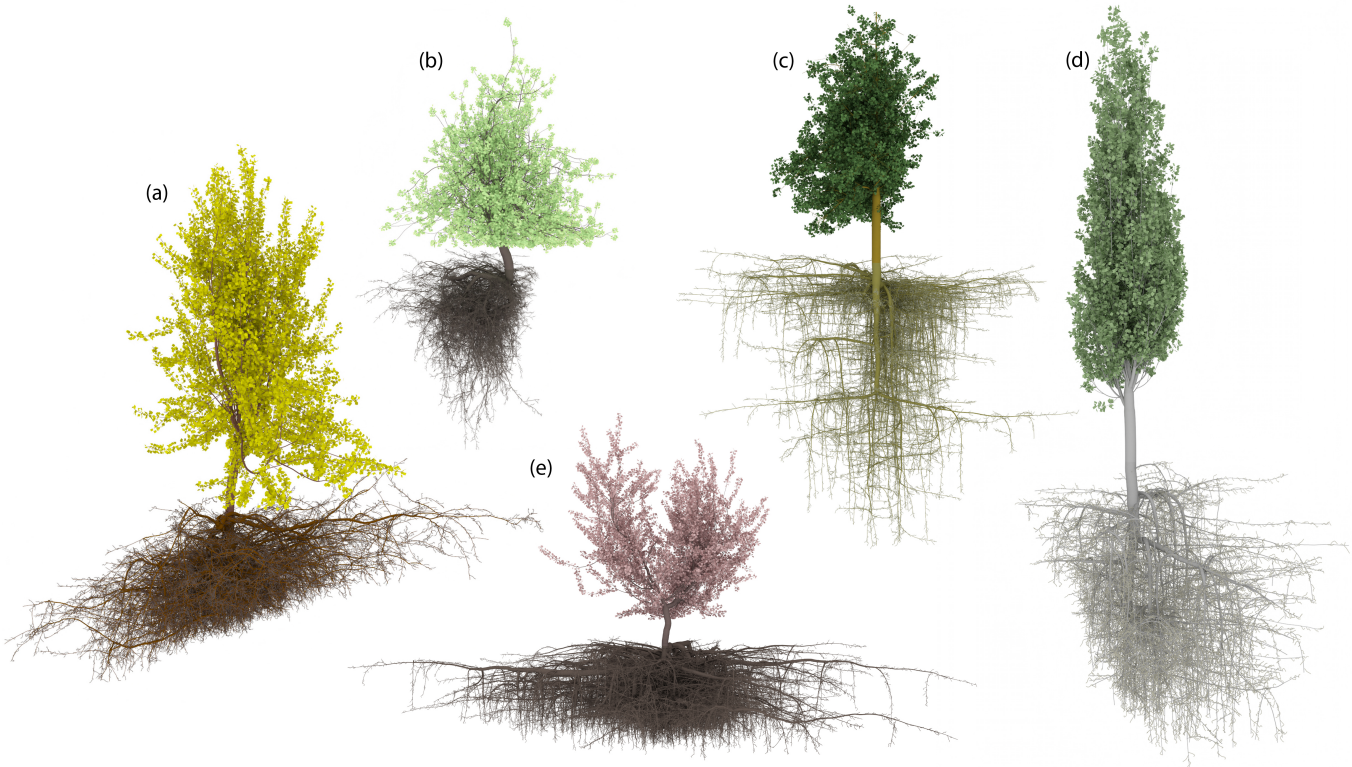

Fig. 12. We demonstrate the capabilities of our method by generating five tree species by manually selecting parameter values: a maple grown on a slope (a), an apple tree grown next to a low permeability region (b), an oak with a deep taproot (c), a poplar with a root distinct from the shoot architecture (d), and a cherry tree with a wide lateral root system (e). Trees can develop different root systems based on their parametrization and the interaction with soil properties.

(e). For a comparison to our simulation, we show a reconstruction of a real root system in Fig. 13 (Fig. 4 in Danjon and Reubens [2008], Species: P. pinaster). Finally, to illustrate our simulated root shapes from a different viewpoint, we show top-down views of two root systems in Fig. 17.

8.1.1 Root-Soil Interaction. Roots are plastic organs that adapt to environmental stimuli. We show that our method captures this important aspect of root development in Fig. 11. We placed a plant model on the slope of a hill. Since root development is affected by nutrients that are only located in the soil (see Eqs. 6, 24), the generated root geometry follows closely the slope of the terrain. This creates the appearance of roots partially sticking out of the ground, which is a commonly observed feature of real tree growth and an important visual asset for rendering scenes containing trees.

In our model, we can set varying values for soil properties. Especially important for root development is the growth resistance factor δ since it impacts the growth rate of root branches. In Fig. 14, we show the same tree model grown on soils with a heterogeneous growth resistance distribution. In (a), a thin layer of soil with low growth resistance is placed on top of a reddish layer of high growth resistance. The root architecture exhibits an asymmetric shape due to avoiding the high growth resistance soil layer. In (b), the low growth resistance layer is thicker compared to the other scene. As a result, the root branches grow faster into a more spherical and less dense shape. Due to the feedback between root and shoot growth,

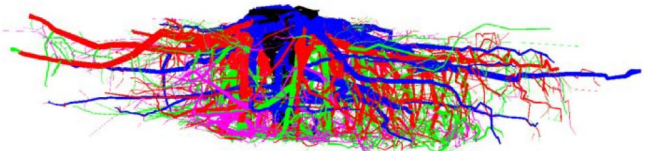

Fig. 13. A reconstruction of a real root system shown in Danjon et al. [2008] (Fig. 4 in their paper). Real trees often develop complex root systems with dense branch distributions. As shown in Fig. 12e, our method is able to generate root systems with similar visual features.

the shape of the above-ground part of the tree is also different from the one shown in scene (a); it grows slightly faster, forming a more well-defined trunk.

To further illustrate the dependence of root development on soil properties, we also evaluated the impact of dynamic soil properties of water capacity and permeability. We map these properties to different soil types as defined by the soil texture triangle (introduced in Sec. 6) to provide a visual, comparative analysis in Fig. 15. The vertical axis indicates varying values for water capacity and permeability, whereas the horizontal axis indicates root development over time. In sandy clay loam (a), the tree first develops a pronounced taproot but later switches to a lateral root system. In silt loam (b), the same tree produces a pronounced tap root system because nutrients infiltrate deeper into the soil compared to sandy clay loam soil. Clay soils (c) are characterized in our simulation by very slow water flow

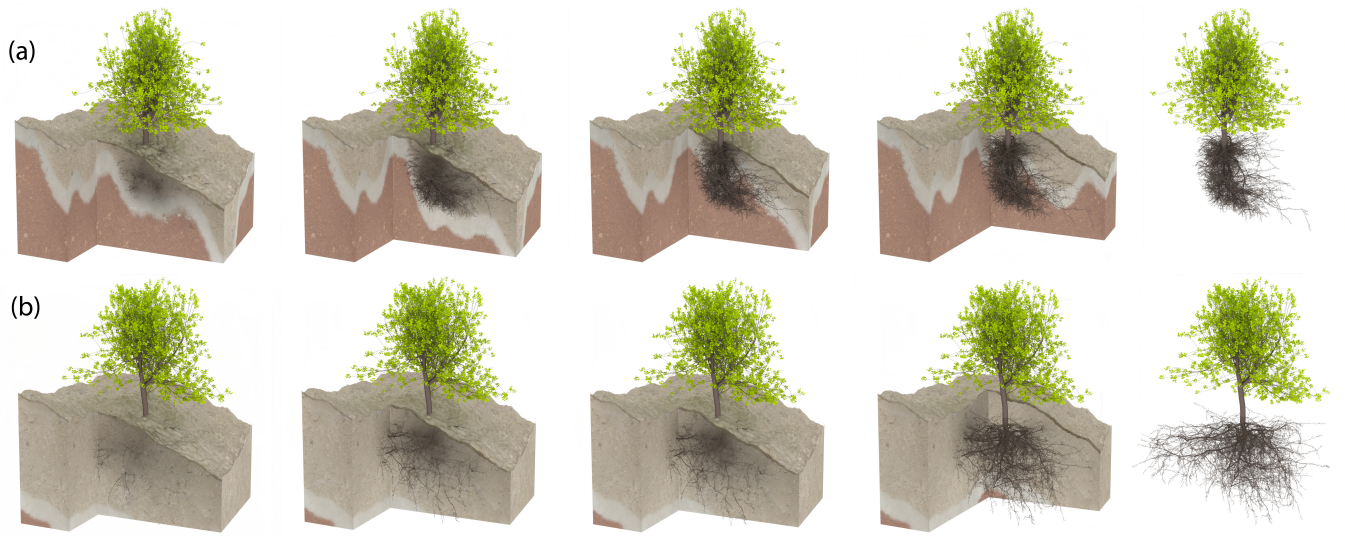

Fig. 14. A visualization of the interaction of the same plant species and two different kinds of soil. The top row (a) illustrates the development of a tree model in soil with a thin layer of low growth resistance properties and the bottom row (b) the development of a tree model in soil with a thick layer of low growth resistance properties. In the latter case, the root branches grow longer and develop into a more spherical shape compared to the former case, where the high growth resistance bottom layer constraints root growth.

characteristics resulting in high nutrient concentrations close to the surface. As a result, the same tree develops a lateral root system.

8.2 Evaluation

We evaluated our tree model qualitatively and quantitatively by assessing the similarity of generated roots to observations of real root systems. Most scientific research focuses on observations of small flowering plants such as Arabidopsis thaliana and not trees, as is the focus of our method. We compare our results with quantitative measurements of oak roots, qualitatively with a root penetration depth of different tree species, and by comparing to the nitrate response of a split root experiment. Furthermore, we also provide examples of the runtime of our method for different simulation time steps and trees in Table 3 of the Appendix.

8.2.1 Root-Shoot Ratio. Trees are known to have different root-to-shoot ratios throughout their development. This progression of ratios is particularly pronounced for oak trees that usually develop a tap root system. Therefore, we compare the development of a simulated oak tree to a real oak tree [Konôpka et al. 2010]. In the inset figure, we show the root-to-shoot ratio as a function of the diameter at the base of the tree of a simulated tree (blue) and a real tree (orange). Our method generates a root-to-shoot distribution similar to the real oak tree. A naive simulation approach of adding a root growth model without coordination with a shoot growth model would not allow to easily produce specific shoot-to-root ratios.

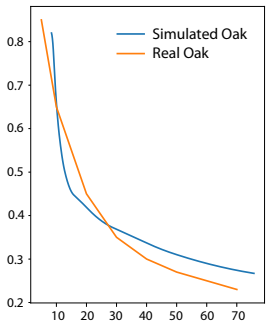

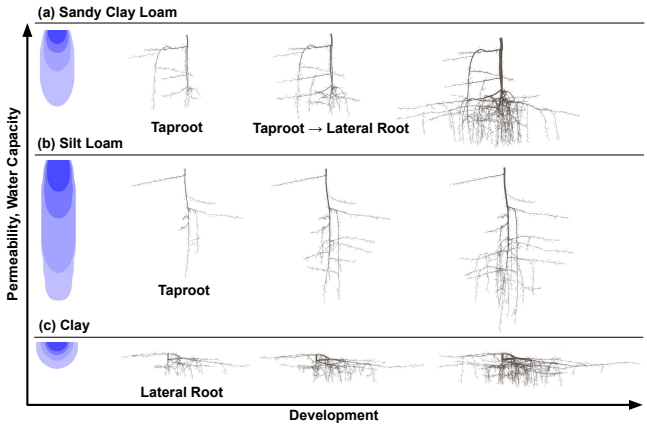

Fig. 15. In our model, trees express different root architectures in soils with different properties. We demonstrate this dependence by developing the same tree species (defined by the same parameter value configuration) in three different types of soils. We use the parameterization for sandy clay loam (a), silt loam (b), and clay (c).

8.2.2 Split Root. Plant root development is highly dependent on nitrate availability in the soil. Nitrate acts as a resource for the growth and can limit growth in case there is not enough nitrate available (Fig.16a). When nitrate levels are too high the plant can repress the growth of the root, since optimal nitrate uptake is facilitated also with a smaller root system (Fig.16b). However, in a scenario where a part of the root system is in high nitrate conditions while the other part is in low nitrate conditions a competition of root branch growth may occur. This competitive root growth is hypothesized to be the result of long-distance signaling between shoot and root system [Boer et al. 2020]. In this asymmetric nitrate distribution scenario the root branches in the high nitrate conditions develop even more vigorously compared to the case when the whole root

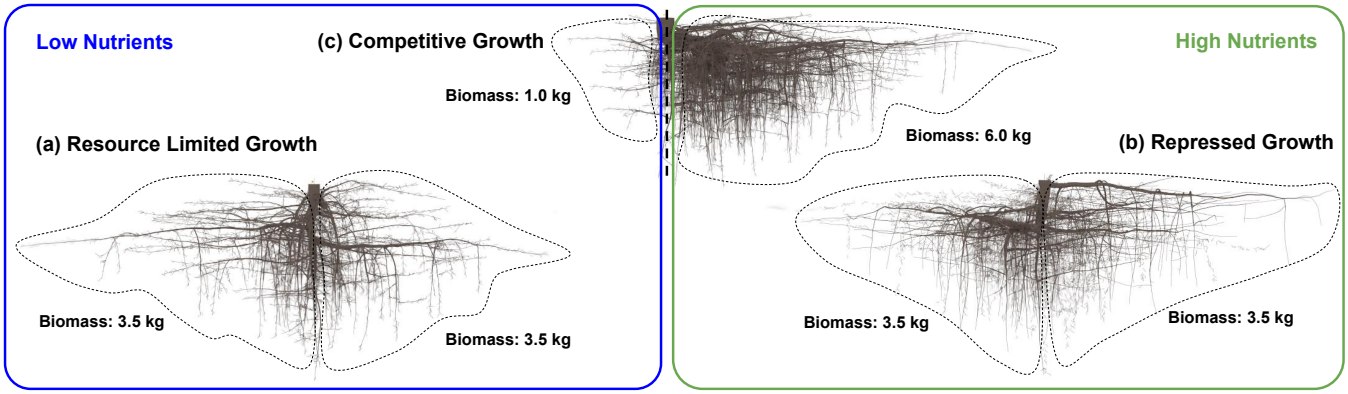

Fig. 16. Nutrients may have intricate effects on root development. In low nutrient regimes, root system development may be limited (a). Whereas, in high nutrient regimes, the root system might develop in a repressed way because further investment in root biomass might be unnecessary to obtain optimal resource requirement (b). In case part of the root system is embedded in high and another part in low nutrient regions, an asymmetric competition scenario arises. The root branches in higher nutrient regions develop faster at the expense of the root branches embedded in lower nutrient regions (c).

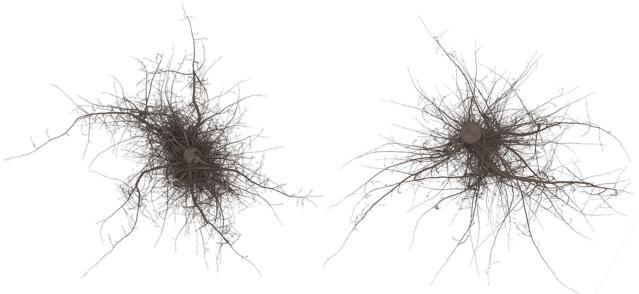

Fig. 17. Top-down views of two root systems: if not blocked by obstacles root systems naturally develop in all radial directions.

system is embedded in high nitrate conditions. Conversely, the root branches which are exposed to low nitrate conditions develop slower compared to the control experiment (Fig.16c). This means that our model based on long-distance signaling can reproduce intricate developmental responses of roots to nitrate distributions. In Fig. 19 we show a rendering of a tree grown close to a nutrient pocket (terracotta region) that further illustrates the asymmetric competition between root branches induced by heterogeneous nutrient distribution. The left part of the root system contains more branches compared to the right part due to a higher activation probability $P_{RA}(rb)$ (Eq. 24).

8.3 Discussion and Limitations

Modeling the 3D geometric development of roots has not received much attention in computer graphics or in other research areas for that matter. The main reason is not the lack of significance of this developmental phenomenon but rather that most of the root system cannot be directly observed. Root systems embedded in soil have to be scanned with X-ray computer tomography (X-Ray CT) or magnetic resonance imaging (MRI) which is observation expensive. As a result, human understanding of how developmental processes are controlled by biology is limited. This complicates formulating and formalizing hypotheses of the development of root systems. In our method this is reflected, e.g., by the modeling decision that root tropism is to a large degree a random process (see Eq. 23). While this does not noticeably affect the expressive capabilities of our modeling approach, a more thorough evaluation of potential hypotheses may lead to a more accurate simulation.

On the other hand, work in developmental biology indicates a number of plant signals that seem important in root growth, e.g., auxin, sugar and nitrate. Currently, our framework based on long-distance signaling reflects certain plant signal actions, such as bud activation being inhibited by buds higher up in the plant structure, which is known to be attributed to the action of auxin flow. However, we refrained to tie in closer to actual plant signaling dynamics due an increased model and computational complexity. A more realistic model would describe signaling dynamics more accurately, which could lead to the emergent description of other important plant developmental phenomena such as adventitious bud formation or a plausible wounding response.

9 CONCLUSION AND FUTURE WORK

We have advanced plant modeling in computer graphics by introducing a novel method for simulating the coordinated development of shoot and root systems. We extend existing methods for the light-mediated generation of plant models by introducing a hierarchical graph representation for the information processing between shoots and roots. The long-distance signaling between roots and shoots not only enables – for the first time – to generate complete models of trees but also to emergently grow complex root systems with known root types, such as tap roots, heart roots, lateral roots, and sinker roots.

A developing root system interacts with soil and dynamically adjusts to varying soil properties as well as nutrient and water gradients. Through numerous examples, we have shown that our method is able to enhance the visual realism of tree models significantly. Furthermore, we have validated our results based on three experiments: root development in different soil types, root-to-shoot ratio, and the split root experiment. This indicates that our method is able to model root development with a high degree of realism.

A model for the plant growth of complete trees enables multiple avenues for future work. For one, it seems interesting to further

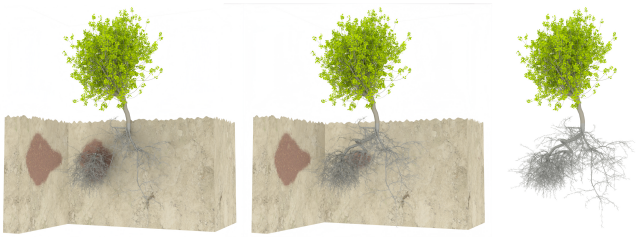

Fig. 18. A tree model grown in soil with a nutrient pocket (terracotta region) exhibits an asymmetric root architecture. As a consequence, on the left side of the root system there are more root branches compared to the right. These results conform to the ones shown in Fig. 16.

Fig. 19. Regions in the soil with high growth resistance represent obstacles for root growth. A tree model is growing around such a region indicated by the terracotta color. This results in an asymmetric root shape.

increase the realism of our procedural models and the interaction of roots with soil. Our current model does not consider physical root-root interactions. Resolving these interactions, also considering root-soil collisions, is challenging. However, it is expected that resolving these interactions would further increase the realism of the generated roots. Second, it would be interesting to calibrate our model with measurements of real roots. While this is a challenging effort – captures of real root systems are inherently difficult to obtain – a more carefully calibrated model would likely be useful to understand root systems further and to develop new hypotheses for tree growth. Third, a model for tree development that also considers root systems and the response of trees to water and nutrient gradients can be useful for applications in urban planning and agriculture to predict the development of trees more realistically.

ACKNOWLEDGMENTS

This research was supported by the Foundation for Food and Agriculture Research, United States Grant ID: 602757 to Benes. The content of this publication is solely the responsibility of the authors and does not necessarily represent the official views of the Foundation for Food and Agriculture Research. This project was also sponsored by USDA NIFA, Award #2023-68012-38992 grant "Promoting Economic Resilience and Sustainability of the Eastern U.S. Forests" to Benes. This work has also been partially supported by KAUST individual baseline funding. We thank the reviewers for their suggestions to improve our work.

REFERENCES

F. Anastacio, M. C. Sousa, F. Samavati, and J. A. Jorge. 2006. Modeling Plant Structures Using Concept Sketches *(NPAR '06)*. ACM, 105–113.

M. Aono and T.L. Kunii. 1984. Botanical Tree Image Generation. *IEEE Comput. Graph. Appl.* 4(5) (1984), 10–34.

O. Argudo, A. Chica, and C. Andujar. 2016. Single-picture Reconstruction and Rendering of Trees for Plausible Vegetation Synthesis. *Comput. Graph.* 57, C (2016), 55–67.

P. Becker and A. Castillo. 1990. Root Architecture of Shrubs and Saplings in the Understory of a Tropical Moist Forest in Lowland Panama. *Biotropica* 22, 3 (1990), 242–249.

B. Benes, N. Andrysco, and O. Šťava. 2009. Interactive Modeling of Virtual Ecosystems. In *Proceedings of the Fifth Eurographics Conference on Natural Phenomena* (Munich, Germany) *(NPH'09)*. Eurographics Association, Goslar, DEU, 9–16.

T Berleth and T Sachs. 2001. Plant morphogenesis: long-distance coordination and local patterning. *Curr. Opin. Plant Biol.* 4, 1 (Feb. 2001), 57–62.

G. Biddle. 2001. Tree Root Damage to Buildings. (2001), 1–23.

M. D. Boer, J. Santos Teixeira, and K. H. Ten Tusscher. 2020. Modeling of Root Nitrate Responses Suggests Preferential Foraging Arises From the Integration of Demand, Supply and Local Presence Signals. *Frontiers in Plant Science* 11 (2020).

D. Bradley, D. Nowrouzezahrai, and P. Beardsley. 2013. Image-based Reconstruction and Synthesis of Dense Foliage. *ACM TOG* 32, 4, Article 74 (2013), 74:1–74:10 pages.

M. Busgen. 2007. *The Structure and Life of Forest Trees.* Read Books.

X. Chen, B. Neubert, Y.-Q. Xu, O. Deussen, and S. B. Kang. 2008. Sketch-Based Tree Modeling Using Markov Random Field. *ACM TOG* 27, 5, Article 109 (Dec. 2008).

G. Cordonnier, E. Galin, J. Gain, B. Benes, E. Guérin, A. Peytavie, and M.-P. Cani. 2017. Authoring Landscapes by Combining Ecosystem and Terrain Erosion Simulation. *ACM Trans. Graph.* 36, 4, Article 134 (July 2017), 12 pages.

M. P. Coutts. 1987. Developmental processes in tree root systems. *Canadian Journal of Forest Research* 17, 8 (1987), 761–767.

M. P. Coutts. 1989. Factors affecting the direction of growth of tree roots. *Ann. For. Sci.* 46 (1989), 277s–287s.

D. F. Cutler, P. E. Gasson, and M. C. Farmer. 1990. The Wind Blown Tree Survey: Analysis of Results. *Arboricultural Journal* 14, 3 (1990), 265–286.

F. Danjon and B. Reubens. 2008. Assessing and analyzing 3D architecture of woody root systems, a review of methods and applications in tree and soil stability, resource acquisition and allocation. *Plant and Soil* 303, 1 (01 Feb 2008), 1–34.

M. Dobson, Arboricultural Advisory, and Information Service (Great Britain). 1995. *Tree Root Systems.* Arboricultural Advisory & Information Service.

P. Ecormier-Nocca, G. Cordonnier, P. Carrez, A.-M. Moigne, P. Memari, B. Benes, and M.-P. Cani. 2021. Authoring Consistent Landscapes with Flora and Fauna. *ACM Trans. Graph.* 40, 4 (2021).

P. E. Gasson and D. F. Cutler. 1990. Tree Root Plate Morphology. *Arboricultural Journal* 14, 3 (1990), 193–264.

E. F. Gilman. 1990. Tree Root Growth and Development. I. Form, Spread, Depth and Periodicity. *Journal of environmental horticulture* 8 (1990), 215–220.

N. Greene. 1991. Detailing Tree Skeleton with Voxel Automata. *SIGGRAPH'91, Course Notes on Photorealistic Volume Modeling and Rendering Techniques* (1991).

D. Groenendyk, T. Ferré, K. Thorp, and A. Rice. 2015. Hydrologic-Process-Based Soil Texture Classifications for Improved Visualization of Landscape Function. *PloS one* 10 (06 2015), e0131299.

J. Guo, H. Jiang, B. Benes, O. Deussen, X. Zhang, D. Lischinski, and H. Huang. 2020. Inverse Procedural Modeling of Branching Structures by Inferring L-Systems. *ACM TOG* 39, 5, Article 155 (June 2020), 13 pages.

R. Habel, A. Kusternig, and M. Wimmer. 2009. Physically Guided Animation of Trees. *CGF* 28, 2 (2009), 523–532.

T. Hädrich, D. T. Banuti, W. Pałubicki, S. Pirk, and D. L. Michels. 2021. Fire in Paradise: Mesoscale Simulation of Wildfires. *ACM Trans. Graph.* 40, 4, Article 163 (July 2021).

T. Hädrich, B. Benes, O. Deussen, and S. Pirk. 2017. Interactive Modeling and Authoring of Climbing Plants. *Comput. Graph. Forum* 36, 2 (May 2017), 49–61.

E. J. Hodgkins and N. G. Nichols. 1977. Extent of Main Lateral Roots in Natural Longleaf Pine as Related to Position and Age of the Trees. *Forest Science* 23, 2 (06 1977), 161–166.

H. Honda. 1971. Description of the form of trees by the parameters of the tree-like body: Effects of the branching angle and the branch length on the shape of the tree-like body. *Journal of Theoretical Biology* 31, 2 (1971), 331 – 338.

T. Ijiri, S. Owada, and T. Igarashi. 2006. Seamless Integration of Initial Sketching and Subsequent Detail Editing in Flower Modeling. *CGF* 25, 3 (2006), 617–624.

J. Klein, R. E. Waller, S. Pirk, W. Pałubicki, M. Tester, and D. L. Michels. 2023. Synthetic Data at Scale: A Paradigm to Efficiently Leverage Machine Learning in Agriculture. *SSRN 4314564* (2023).

B. Konôpka, J. Pajtík, M. Moravčík, and M. Lukac. 2010. Biomass partitioning and growth efficiency in four naturally regenerated forest tree species. *Basic and Applied Ecology* 11, 3 (2010), 234–243.

J. Kratt, Mark Spicker, A. Guayaquil, M. Fišer, S. Pirk, O. Deussen, J. C. Hart, and B. Benes. 2015. Woodification: User-Controlled Cambial Growth Modeling. *CGF* 34, 2 (2015), 361–372.

D. Leitner, S. Klepsch, G. Bodner, and A. Schnepf. 2010. A dynamic root system growth model based on L-Systems. *Plant and Soil* 332, 1 (01 Jul 2010), 177–192.

O. Leyser. 2011. Auxin, Self-Organisation, and the Colonial Nature of Plants. *Current Biology* 21, 9 (2011), R331–R337.

B. Li, J. Kałużny, J. Klein, D. L. Michels, W. Pałubicki, B. Benes, and S. Pirk. 2021. Learning to Reconstruct Botanical Trees from Single Images. *ACM Transaction on Graphics* 40, 6, Article 231 (12 2021).
C. Li, O. Deussen, Y.-Z. Song, P. Willis, and P. Hall. 2011. Modeling and Generating Moving Trees from Video. *ACM TOG* 30, 6, Article 127 (2011), 127:1–127:12 pages.
Y. Li, X. Fan, N. J. Mitra, D. Chamovitz, D. Cohen-Or, and B. Chen. 2013. Analyzing Growing Plants from 4D Point Cloud Data. *ACM TOG* 32, 6, Article 157 (2013).
Y. Liu, J. Guo, B. Benes, O. Deussen, X. Zhang, and H. Huang. 2021. TreePartNet: Neural Decomposition of Point Clouds for 3D Tree Reconstruction. *ACM Transaction on Graphics* 40, 6, Article 232 (Dec. 2021), 16 pages.
Y. Livny, S. Pirk, Z. Cheng, F. Yan, O. Deussen, D. Cohen-Or, and B. Chen. 2011. Texture-Lobes for Tree Modelling. In *ACM SIGGRAPH 2011 Papers (SIGGRAPH '11)*. ACM, Article 53, 10 pages.
S. Longay, A. Runions, F. Boudon, and P. Prusinkiewicz. 2012. TreeSketch: Interactive Procedural Modeling of Trees on a Tablet. In *Proceedings of the International Symposium on Sketch-Based Interfaces and Modeling (SBIM '12)*. 107–120.
Y. Lu, Y. Wang, Z. Chen, A. Khan, C. Salvaggio, and G. Lu. 2021. 3D plant root system reconstruction based on fusion of deep structure-from-motion and IMU. *Multimedia Tools and Applications* 80, 11 (01 May 2021), 17315–17331.
M. Makowski, T. Hädrich, J. Scheffczyk, D. L. Michels, S. Pirk, and W. Pałubicki. 2019. Synthetic Silviculture: Multi-Scale Modeling of Plant Ecosystems. *ACM Trans. Graph.* 38, 4, Article 131 (July 2019), 14 pages.
E. C. Morris, M. Griffiths, A. Golebiowska, S. Mairhofer, J. Burr-Hersey, T. Goh, D. von Wangenheim, B. Atkinson, C. J. Sturrock, J. P. Lynch, K. Vissenberg, K. Ritz, D. M. Wells, S. J. Mooney, and M. J. Bennett. 2017. Shaping 3D Root System Architecture. *Current Biology* 27, 17 (2017), R919–R930.
R. Měch and P. Prusinkiewicz. 1996. Visual Models of Plants Interacting with Their Environment. In *Proceedings of the 23rd Annual Conference on Computer Graphics and Interactive Techniques (SIGGRAPH '96)*. ACM, 397–410.
B. Neubert, T. Franken, and O. Deussen. 2007. Approximate Image-based Tree-modeling Using Particle Flows. *ACM TOG* 26, 3, Article 88 (2007).
M. Ohashi, H. Ikeno, K. Sekihara, T. Tanikawa, M. Dannoura, K. Yamase, C. Todo, T. Tomita, and Y. Hirano. 2019. Reconstruction of root systems in Cryptomeria japonica using root point coordinates and diameters. *Planta* 249, 2 (2019), 445–455.
M. Okabe, S. Owada, and T. Igarashi. 2007. Interactive Design of Botanical Trees Using Freehand Sketches and Example-based Editing. In *ACM SIGGRAPH Courses* (San Diego, California). ACM, Article 26.
P. E. Oppenheimer. 1986. Real time design and animation of fractal plants and trees. *Proc. of SIGGRAPH* 20, 4 (1986), 55–64.
W. Palubicki, K. Horel, S. Longay, A. Runions, B. Lane, R. Měch, and P. Prusinkiewicz. 2009. Self-Organizing Tree Models for Image Synthesis. *ACM Trans. Graph.* 28, 3, Article 58 (jul 2009), 10 pages.
W. Pałubicki, M. Makowski, W. Gajda, T. Hädrich, D. L. Michels, and S. Pirk. 2022. Ecoclimates: Climate-Response Modeling of Vegetation. *ACM Trans. Graph.* 41, 4, Article 155 (2022), 19 pages.
S. Pirk, M. Jarząbek, T. Hädrich, D. L. Michels, and W. Palubicki. 2017. Interactive Wood Combustion for Botanical Tree Models. *ACM Trans. Graph.* 36, 6, Article 197 (Nov. 2017), 12 pages.
S. Pirk, T. Niese, O. Deussen, and B. Neubert. 2012a. Capturing and animating the morphogenesis of polygonal tree models. *ACM TOG* 31, 6, Article 169 (2012), 169:1–169:10 pages.
S. Pirk, T. Niese, T. Hädrich, B. Benes, and O. Deussen. 2014. Windy Trees: Computing Stress Response for Developmental Tree Models. *ACM TOG* 33, 6, Article 204 (2014), 204:1–204:11 pages.
S. Pirk, O. Stava, J. Kratt, M. A. M. Said, B. Neubert, R. Měch, B. Benes, and O. Deussen. 2012b. Plastic Trees: Interactive Self-adapting Botanical Tree Models. *ACM Trans. Graph.* 31, 4, Article 50 (July 2012), 10 pages.
A Plus. 2023. 3 Types of Tree Root Systems. online. https://aplustree.com/3-types-of-tree-root-systems/
P. Prusinkiewicz. 1986. Graphical applications of L-systems. In *Proc. on Graph. Interf.* 247–253.
P. Prusinkiewicz and Aristid Lindenmayer. 1990. *The Algorithmic Beauty of Plants*. Springer-Verlag New York, Inc.
J. Puig, G. Pauluzzi, E. Guiderdoni, and P. Gantet. 2012. Regulation of Shoot and Root Development through Mutual Signaling. *Molecular plant* 5 (05 2012), 974–83.
L. Quan, P. Tan, G. Zeng, L. Yuan, J. Wang, and S. B. Kang. 2006. Image-Based Plant Modeling. *ACM TOG* 25, 3 (July 2006), 599–604.
E. Quigley, Y. Yu, J. Huang, W. Lin, and R. Fedkiw. 2018. Real-Time Interactive Tree Animation. *IEEE TVCG* 24, 5 (2018), 1717–1727.
A. Reche-Martinez, I. Martin, and G. Drettakis. 2004. Volumetric reconstruction and interactive rendering of trees from photographs. *ACM TOG* 23, 3 (2004), 720–727.
W. T. Reeves and R. Blau. 1985. Approximate and Probabilistic Algorithms for Shading and Rendering Structured Particle Systems. *SIGGRAPH Comput. Graph.* 19, 3 (July 1985), 313–322.
A. Runions, B. Lane, and P. Prusinkiewicz. 2007. Modeling Trees with a Space Colonization Algorithm. *EG Nat. Phenom.* (2007), 63–70.
H. Shao, T. Kugelstadt, T. Hädrich, W. Pałubicki, J. Bender, S. Pirk, and D. L. Michels. 2021. Accurately Solving Rod Dynamics with Graph Learning. In *NeurIPS*.
K. Shinozaki, K. Yoda, K. Hozumi, and T. Kira. 1964. A quantitative analysis of plant form - the pipe model theory I. Basic analysis. *Japanese Journal of Ecology* 14 (1964), 97–104. Issue 3.
O. Stava, S. Pirk, J. Kratt, B. Chen, R. Měch, O. Deussen, and B. Benes. 2014. Inverse Procedural Modelling of Trees. *Computer Graphics Forum* (2014), n/a–n/a.
E. L. Stone and P. J. Kalisz. 1991. On the maximum extent of tree roots. *Forest Ecology and Management* 46, 1 (1991), 59–102.
B.B. Stout. 1956. *Studies of the Root Systems of Deciduous Trees*. Black Rock Forest.
R. F. Sutton. 1980. Root system morphogenesis. *NZJ For. Sci* 10, 1 (1980), 264–292.
R. F. Sutton. 1991. Soil properties and root development in forest trees: a review. *Information report OX-Canadian Forestry Service, Great Lakes Forestry Centre* (1991).
P. Tan, T. Fang, J. Xiao, P. Zhao, and L. Quan. 2008. Single Image Tree Modeling. *ACM TOG* 27, 5, Article 108 (2008), 7 pages.
B. Tobin, J. Čermák, D. Chiatante, F. Danjon, A. Di Iorio, L. Dupuy, A. Eshel, C. Jourdan, T. Kalliokoski, R. Laiho, N. Nadezhdina, B. Nicoll, L. Pagès, J. Silva, and I. Spanos. 2007. Towards developmental modelling of tree root systems. *Plant Biosystems - An International Journal Dealing with all Aspects of Plant Biology* 141, 3 (2007), 481–501.
G. Vercambre, L. Pagès, C. Doussan, and R. Habib. 2003. Architectural analysis and synthesis of the plum tree root system in an orchard using a quantitative modelling approach. *Plant and Soil* 251, 1 (01 Apr 2003), 1–11.
B. Wang, Y. Zhao, and J. Barbič. 2017. Botanical Materials Based on Biomechanics. *ACM Trans. Graph.* 36, 4, Article 135 (2017).
J. Wither, F. Boudon, M.-P. Cani, and C. Godin. 2009. Structure from silhouettes: a new paradigm for fast sketch-based design of trees. *CGF* 28, 2 (2009), 541–550.
S.-K. Wong and K.-C. Chen. 2015. A Procedural Approach to Modelling Virtual Climbing Plants With Tendrils. *Comput. Graph. Forum* (2015).
H. Xu, N. Gossett, and B. Chen. 2007. Knowledge and heuristic-based modeling of laser-scanned trees. *ACM TOG* 26, 4 (2007), Article 19, 13 pages.
Y. Zhao and J. Barbič. 2013. Interactive Authoring of Simulation-ready Plants. *ACM TOG* 32, 4, Article 84 (2013), 12 pages.

APPENDIX

Glossary

Acropetal	Upward from the base or the point of attachment.
Apical bud	The bud located at the end of a branch, which is the location where shoot growth occurs.
Apical control	is the inhibition of lateral branch growth by shoots above it (distal shoots). If the distal shoots are cut off to remove apical control, the lateral branch can grow larger and may bend upwards.
Apical dominance	is the inhibition of lateral bud growth by buds above it (distal buds). If the distal buds are cut off to remove apical dominance, the lateral bud can grow out.
Basipetal	Downward toward the base or point of attachment.
Lateral bud	A lateral or axillary bud is located in the axil of a leaf. Each bud has the potential to form shoots, and may be specialized in producing either vegetative shoots (stems and branches) or reproductive shoots (flowers).
Morphology	the study of the form and structure of organisms and their specific structural features.
Root	A branch typically sprouting from the underground stock of a plant which attaches it to the soil.
Shoot	A young branch sprouting from the aboveground stock of a plant.
Tropism	the turning of all or part of an organism in a particular direction in response to an external stimulus. Phototropism: growth of a plant in response to a light. Gravitropism: growth of a plant in response of gravity.
Vigor	is the vitality of a plant and its subsequent performance.

List of Symbols

G	maximum growth requirement of node
M	maintenance growth requirement
A	bud activation signal
R	root competition signal
S	shoot competition signal
l	internode length
d	internode diameter
L	light availability
S_F	shoot flux
R_F	root flux
w	soil water
v	soil nutrients
δ	soil growth resistance factor
c	soil water capacity
p	soil permeability
α	soil water content
$\mathcal{S}$	a source/sink
f_{diff}	diffusion force
f_{grav}	gravity
q	light value calculated from sampling the RBV
V	vigor of nodes
shoot_g	growth potential of shoot
root_g	growth potential of root
N_b	bud number
N_l	leaf number
T	day temperature
sb	shoot bud
rb	root bud
$P_A(sb)$	probability to activate shoot bud
$P_T(n)$	probability to switch between lateral- and gravitropism
$P_{rb}(n)$	probability to activate root bud
τ	tropism vector
ζ	tropism vector weight
γ	optimal growth direction vector
η	optimal growth direction vector weight
φ_{BA}	bud activation coefficient
φ_{PT}	pruning threshold
φ_{ST}	global probability to switch tropism
φ_{STD}	local probability to switch tropism
φ_{NLB}	number of buds produced
φ_{AC}	capacity of apical nodes to control growth of other nodes
φ_{RG}	root growth rate
φ_{ACD}	capacity of apical nodes to control activation of buds
φ_{BS}	branching strength
φ_{SD}	signal decay
$n \in N$	node in segment graph
$b \in B$	node in branch graph
N	segment graph
B	branch graph
P	global plant state
ρ	tree age

Simulation Time

Table 3. Computation times in seconds for simulations with time steps of 1 day, 1 week, and 1 month (rows) for trees with varying node counts ranging from 10k to 60k (columns). Simulations with monthly time steps can be computed at interactive rates at all levels of plant structure complexity.

Time step	**10k**	**20k**	**30k**	**40k**	**60k**
1 day	15.4s	32.5s	46.9s	62.4s	93.7s
1 week	2.1s	4.3s	6.2s	8.3s	12.5s
1 month	0.45s	0.91s	1.37s	1.82s	2.73s

Parameter Values

Table 4. A list of parameter values for each species used to generate the results shown in Figure 12.

Parameters	**Cherry**	**Apple**	**Oak**	**Poplar**	**Maple**
δ	1.0	0.5	0.1	0.3	1.0
φ_{ACD}	3.0	3.0	2.0	1.0	0.5
φ_{RG}	14.5	8.5	12.5	10.0	11.0
τ	0.7	0.05	0.85	0.65	0.1
φ_{ST}	0.95	1.0	0.6	0.75	1.0
φ_{STD}	0.01	0.02	0.01	0.07	0.0
φ_{SD}	1.0	0.9	0.95	0.99	0.95
N_b	2	2	1	2	1
N_l	1	1	1	1	1
φ_{ACD}	0.0	4.0	1.0	0.5	1.0
l	0.03	0.03	0.04	0.03	0.03
φ_{AC}	0.0	-0.03	0.1	0.25	0.15
τ	0.04	0.01	0.02	0.03	0.05
φ_{SD}	0.99	0.91	0.85	0.96	1.0
φ_{PT}	0.05	0.03	0.01	0.0	0.02